cmgh
CELLULAR AND MOLECULAR GASTROENTEROLOGY AND HEPATOLOGY

ORIGINAL RESEARCH

Enteropathogenic *Escherichia coli* EspH-Mediated Rho GTPase Inhibition Results in Desmosomal Perturbations

Jennifer Lising Roxas,[1] Ross Calvin Monasky,[1] Bryan Angelo P. Roxas,[1] Al B. Agellon,[1,2] Asad Mansoor,[1] James B. Kaper,[3] Gayatri Vedantam,[1,2,4,5,§] and V. K. Viswanathan[1,2,4,§]

[1]*School of Animal and Comparative Biomedical Sciences,* [2]*BIO5 Institute for Collaborative Research,* [4]*Department of Immunobiology, University of Arizona, Tucson, Arizona;* [3]*University of Maryland School of Medicine, Baltimore, Maryland;* [5]*Southern Arizona VA Healthcare System, Tucson, Arizona*

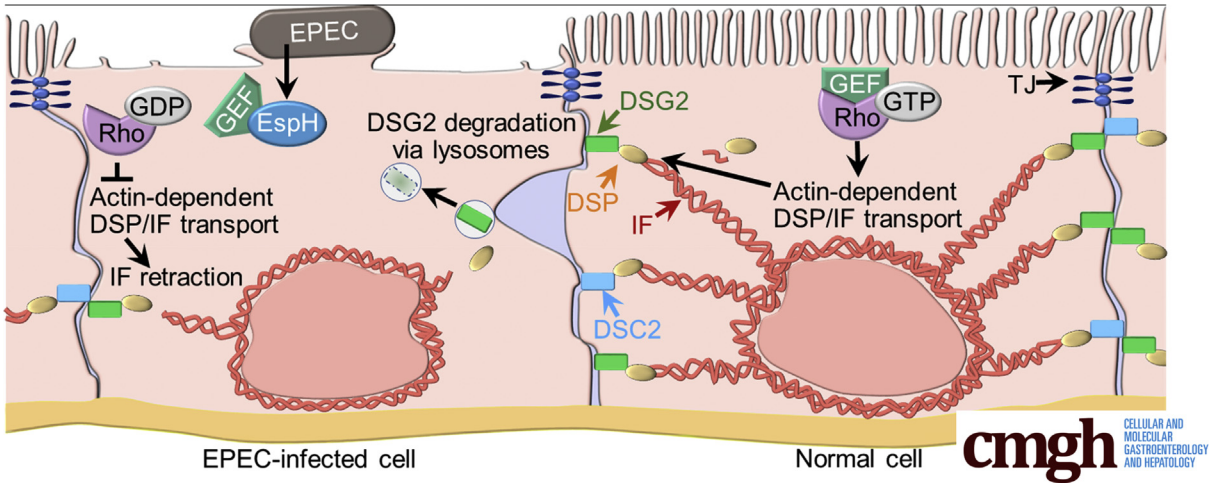

SUMMARY

EspH, a protein secreted by the diarrheagenic pathogen enteropathogenic *Escherichia coli* into intestinal epithelial cells, sequesters Rho guanine nucleotide exchange factors and inhibits Rho guanosine triphosphatases. These EspH effects cause desmosomal perturbations and loss of epithelial barrier integrity, and contribute to bacterial persistence in the intestine.

BACKGROUND & AIMS: The diarrheagenic pathogen, enteropathogenic *Escherichia coli* (EPEC), uses a type III secretion system to deliver effector molecules into intestinal epithelial cells (IECs). While exploring the basis for the lateral membrane separation of EPEC-infected IECs, we observed infection-induced loss of the desmosomal cadherin desmoglein-2 (DSG2). We sought to identify the molecule(s) involved in, and delineate the mechanisms and consequences of, EPEC-induced DSG2 loss.

METHODS: DSG2 abundance and localization was monitored via immunoblotting and immunofluorescence, respectively. Junctional perturbations were visualized by electron microscopy, and cell–cell adhesion was assessed using dispase assays. EspH alanine-scan mutants as well as pharmacologic agents were used to evaluate impacts on desmosomal alterations. EPEC-mediated DSG2 loss, and its impact on bacterial colonization in vivo, was assessed using a murine model.

RESULTS: The secreted virulence protein EspH mediates EPEC-induced DSG2 degradation, and contributes to desmosomal perturbation, loss of cell junction integrity, and barrier disruption in infected IECs. EspH sequesters Rho guanine nucleotide exchange factors and inhibits Rho guanosine triphosphatase signaling; EspH mutants impaired for Rho guanine nucleotide exchange factor interaction failed to inhibit RhoA or deplete DSG2. Cytotoxic necrotizing factor 1, which locks Rho guanosine triphosphatase in the active state, jasplakinolide, a molecule that promotes actin polymerization, and the lysosomal inhibitor bafilomycin A, respectively, rescued infected cells from EPEC-induced DSG2 loss. Wild-type EPEC, but not an *espH*-deficient strain, colonizes mouse intestines robustly, widens paracellular junctions, and induces DSG2 re-localization in vivo.

CONCLUSIONS: Our studies define the mechanism and consequences of EPEC-induced desmosomal alterations in IECs. These perturbations contribute to the colonization and virulence of EPEC, and likely related pathogens. *(Cell Mol Gastroenterol Hepatol 2018;6:163–180; https://doi.org/10.1016/j.jcmgh.2018.04.007)*

Keywords: EPEC; Desmoglein; DSG2; Host–Pathogen Interaction.

See editorial on page 225.

The intestinal epithelial monolayer facilitates absorption of nutrients and fluids, and, simultaneously, serves as a barrier against the entry of harmful intraluminal components such as bacteria and toxins into the underlying tissue.[1] The paracellular space between adjacent intestinal epithelial cells (IECs) is bridged by protein complexes including tight junctions (TJs), adherens junctions, gap junctions, and desmosomal junctions.[2]

The apical-most TJs act as fences that maintain polarity by separating apical and basolateral membrane components of the epithelium, and form the major paracellular barrier.[3] Adherens junctions, located immediately below TJs, comprise transmembrane cadherins and cytoplasmically attached α- and β-catenins that connect to cytoskeletal actin filaments.[4] Desmosomal junctions, comprising membrane-anchored desmoglein (DSG) and desmocollin (DSC), form spot-welds that confer stability and strength to cell junctions. Four DSG (DSG1–4) and 3 DSC (DSC1–3) isoforms are expressed in human beings in a tissue-specific manner.[5] Only DSG2 and DSC2 are expressed in normal human intestinal epithelium.[6] The N-termini of DSG and DSC are located in the intercellular space, and form homotypic and heterotypic interactions with desmosomal cadherins of adjacent cells.[7] The plaque proteins plakoglobin, plakophilin, and desmoplakin connect the C-termini of DSG and DSC to intermediate filaments (IFs).[8] Many disease states are marked by relocalization of junctional proteins, increased paracellular permeability, loss of cell–cell adhesion, and, in extreme cases, the gross exfoliation of cells.[9]

Enteropathogenic *Escherichia coli* (EPEC) is a leading cause of juvenile diarrheal disease mortality.[10] EPEC belongs to the attaching and effacing (A/E) family of pathogens that intimately attach to epithelial cells and efface brush-border microvilli.[11] EPEC elaborates a type III secretion system (T3SS) that translocates effector proteins into host cells and thereby modulates host cell signaling. Notably, effector protein-dependent barrier perturbation is thought to contribute to EPEC-induced diarrhea.[12] The EPEC effectors EspF, EspG1/G2, Map, and NleA disrupt TJs and compromise epithelial barrier function.[13–17] EPEC outer-membrane proteins disrupt adherens junctions by inducing the dissociation of cadherin/β-catenin complexes.[18]

Early electron microscopy studies on small intestinal biopsy samples from EPEC-infected children showed a separation of the lateral intercellular junctions of epithelial cells.[19] We observed similar widening of paracellular junctions in EPEC-infected IECs, specifically in regions below the TJs. To test the hypothesis that the loss of desmosomes contributed to these changes, we evaluated desmosomal protein abundance in infected IECs. EPEC infection induced a marked decrease in DSG2, the only IEC desmoglein isoform. The aim of this study, therefore, was to investigate the mechanisms and impact of EPEC-induced DSG2 down-regulation in vitro and in vivo. Our studies show a novel role for the effector protein EspH, and for Rho guanosine triphosphatase (GTPase) signaling, in modulating epithelial monolayer integrity, barrier function, and bacterial colonization.

Materials and Methods

Cell Lines

The human IEC line $C2_{BBe}$, a brush-border–expressing Caco-2 subclone,[20] was used and cultured as reported previously.[21]

Bacterial Strains and Generation of Mutants

The EPEC O127:H6 strain E2348/69 and its isogenic derivatives, and the commensal *E coli* strain HS4, were used (Table 1). E2348/69 *espH* was disrupted via homologous recombination.[22] A 202-bp *espH* internal fragment (base pairs 181–382) was cloned into the suicide vector pJP5603,[23] and the resulting construct, pSE864, was introduced into E2348/69 via conjugation. Transconjugants were confirmed for *espH* disruption by polymerase chain reaction and Southern blot, and 1 representative *espH* mutant, SE874, was used. For complementation studies, full-length *espH* was amplified and cloned into pTrcHis2-TOPO TA (Thermo Fisher Scientific, Waltham, MA) to generate pJLR1, and transformed into SE874 to generate SE874/C. *espH* also was cloned in-frame with the 6XHis tag sequence of pTrcHis2-TOPO TA (pJLR2). Alanine scans have been empirically found to be a particularly effective method for assessing the functional importance of residues within a protein.[24] To identify EspH residues involved in RhoA inhibition, a panel of 29 *espH* alanine-scan mutants were engineered by sequentially replacing 5–amino acid stretches of EspH (excluding the N-terminal 25 amino acids containing the secretion signal) with alanine residues. To facilitate cloning of these mutants, an *Xho*I restriction site was introduced into pJLR2 via a 703G→A silent substitution to generate pJLR4. Dispase assay screens (described later) identified EspH mutants M14 and M16, corresponding to alterations of amino acids 88–92 and 98–102, respectively, as candidates for further study. To verify that M14 and M16 retained wild-type levels of EspH secretion, culture supernatants of wild-type (WT) EPEC and mutant strains grown in serum-free Dulbecco's modified Eagle medium (DMEM) were immunoblotted as described later.

§Authors share co-senior authorship.

Abbreviations used in this paper: **A/E, attaching and effacing; BSA, bovine serum albumin; CM, calcium and magnesium; DMEM, Dulbecco's modified Eagle medium; DSC, desmocollin; DSG, desmoglein; EPEC, enteropathogenic *Escherichia coli*; GEF, guanine nucleotide exchange factors; GTPase, guanosine triphosphatase; IF, intermediate filament; IEC, intestinal epithelial cell; PBS, phosphate-buffered saline; T3SS, type 3 secretion system; TER, transepithelial electrical resistance; TJ, tight junction; WT, wild-type.**

Most current article

2352-345X
https://doi.org/10.1016/j.jcmgh.2018.04.007

Table 1. Bacterial Strains, Plasmids, and Primers

Strain	Genotype/description	Reference
HS4	Nonpathogenic *E coli*	63
EPEC	*E coli* O127:H6 strain E2348/69, Nal^R ; parent strain for all mutants/complements below	64,65
Δ*espA*	Nonpolar insertion in *espA*; Nal^R, Kan^R	66
SE874	Insertional disruption of *espH*; Kan^R, Nal^R	This study
SE874/C	SE874 complemented with pJLR1	This study
Plasmids		
pJP5603	Suicide vector	23
pSE864	pJP5603 with 202-bp insert corresponding to *espH* bp181-382; used for generating SE874	This study
SE874 complementation plasmids: vector: pTrcHis2TOPO-TA		
pJLR1	*espH* amplified with primers EspH1 and EspH2 Expresses WT EspH	This study
pJLR2	*espH* amplified with primers EspH1 and EspH3 Expresses WT EspH with C-terminal 6xHis tag	This study
pJLR4	*espH* with silent mutation at (703G>A) to introduce *Xho*I restriction site Expresses WT EspH with C-terminal 6xHis tag	This study
M14	Alanine-scan mutant Expresses EspH 88AAAAA92, His-tagged	This study
M16	Alanine-scan mutant Expresses EspH 98AAAAA102, His-tagged	This study
Primers		
EspH1	5'-ATGTCGTCATCATTATCAG-3'	This study
EspH2	5'-TTAAACTGTCACACCTGAT-3'	This study
EspH3	5'-AACTGTCACACCTGAT-3'	This study

Growth of Bacteria and Infection of IECs

$C2_{BBe}$ culture medium was changed to serum-free DMEM 16 hours before infection. For infections, overnight bacterial cultures (in Luria–Bertani broth with appropriate antibiotics for plasmid selection) were subcultured at 1:20 dilution in serum-free DMEM and grown to midlogarithmic phase (OD_{600nm}, 0.4) at 37°C. Bacteria were added to the apical surface of IECs corresponding to an initial multiplicity of infection of 100, and infections were allowed to proceed for 3 hours unless otherwise indicated. For studies involving Rho activation or actin polymerization, IECs were pretreated with 300 ng/mL cytotoxic necrotizing factor 1–based Rho activator CN03 (Cytoskeleton, Inc, Denver, CO) or 1 μmol/L jasplakinolide (Thermo Fisher Scientific), for 1 hour before infection. For inhibitor studies, IECs were pretreated with 50 μmol/L pan-caspase inhibitor z-DEVD-fmk, 52 nmol/L calpain inhibitor I, 10 μmol/L proteasomal inhibitor MG132, or 250 nmol/L lysosomal inhibitor bafilomycin A1 (Sigma-Aldrich, St. Louis, MO) for 2 hours before infection, and inhibitor levels were maintained through the course of infection.

Protein Extraction

Mock-treated and infected monolayers were washed with ice-cold, sterile phosphate-buffered saline (PBS) with calcium and magnesium (PBS-CM), scraped, harvested via centrifugation, resuspended in urea buffer (7 mol/L urea, 2 mol/L thiourea, 100 mmol/L 1,4-dithiothreitol, and 4% 3-[(3-Cholamidopropyl)dimethylammonio]-1-propanesulfonate hydrate), and lysed via sonication or by silica bead-beating (Bead Ruptor; Omni International, NW Kennesaw, GA).

Immunoblot Analyses

Protein extracts (50–100 μg) were separated by 7% sodium dodecyl sulfate–polyacrylamide gel electrophoresis, and transferred to 0.2-μm nitrocellulose membranes, which were blocked with 5% nonfat milk in Tris-buffered saline containing Tween 20 and incubated with anti-DSG2, anti-DSC2, or anti-actin antisera (Abcam, Cambridge, MA; Sigma-Aldrich) following product recommendations. Horseradish-peroxidase–conjugated goat anti-rabbit and anti-mouse antisera (Sigma-Aldrich) were used as secondary antisera. Membranes were developed with SuperSignal West Femto Chemiluminescent Substrate (Thermo Fisher Scientific).

Co-immunoprecipitation Studies

$C2_{BBe}$ cells were grown to 60% confluency and transfected with pEnter expression plasmid harboring C-terminal Flag-tagged p115-Rho guanine nucleotide exchange factor (GEF) (Vigene, Rockville, MD). Transfection was facilitated using jetPRIME transfection reagent (Polyplus Transfection, Illkirch, France) following the manufacturer's protocol. Two days after transfection, $C2_{BBe}$ cells were infected with EPEC strains at a multiplicity of infection of 100 for 3 hours. Samples were washed with ice-cold PBS, scraped, and harvested via centrifugation. Proteins were extracted in immunoprecipitation lysis buffer containing 50 mmol/L TrisCl (pH 7.4), 150 mmol/L NaCl, 1 mmol/L EDTA, 1% Nonidet P-40, 0.25% sodium deoxycholate, and 1 × Halt protease and phosphatase inhibitor cocktail (Thermo Fisher Scientific). Immunoprecipitation was

performed on 5-mg protein extracts using Surebeads Protein A Magnetic beads (Bio-Rad Laboratories, Hercules, CA) bound with anti-Flag M2 antibody (Sigma-Aldrich). The presence of Flag-tagged p115-RhoGEF and His-tagged EspH in the immunoprecipitated samples was determined via Western blot analysis using p115-RhoGEF antibody (Abcam) and anti-6xHis-tag antibody (Cell Signaling, Danvers, MA). To assess EspH secretion, 30-mL cultures of EPEC strains inoculated in serum-free DMEM and normalized to midlogarithmic phase (OD_{600nm}, 0.4) were grown for 3 hours at 37°C. Cultures were centrifuged at 400*g* for 10 minutes. Bacterial supernatants were filter-sterilized and concentrated using Amicon 3-kilodalton cut-off filters (MilliporeSigma, Burlington, MA). EspH secretion was assessed via immunoblot analysis using anti-6xHis-tag antibody.

Dispase Assay

Cell adhesion strength was assessed using a modified dispase assay.[25] Briefly, mock-treated and infected IEC monolayers were washed with Hank's balanced salt solution with CM, and incubated with dispase (20 mg/mL in Hank's balanced salt solution with CM) at 37°C and 5% CO_2 for 30 minutes. Detached monolayers were agitated mechanically for 5 minutes, and monolayer disruption was scored qualitatively (none, partial, or full).

RhoA Activity Assays

The low RhoA activity signal under standard infection conditions impeded detection of further EPEC/EspH-mediated inhibition. To overcome this, baseline RhoA activity was boosted by pretreating serum-starved, confluent IECs with 5 μmol/L lysophosphatidic acid for 1 hour before infection. RhoA activity in cell extracts were measured using a RhoA G-LISA Activation Assay Kit (Cytoskeleton, Inc).

Transepithelial Electrical Resistance Measurements

Polarized IECs grown on 0.33-cm^2 collagen-coated Corning Transwells (Thermo Fisher Scientific) were apically infected with EPEC strains (WT, SE874, and SE874/C) cultured in DMEM as described earlier. Measurements were made every hour for 6 hours after infection using an epithelial volt-Ohm voltmeter (World Precision Instruments, Sarasota, FL), and transepithelial electrical resistance (TER) was calculated by applying Ohm's Law.

Mouse Model of EPEC Infection

All procedures were approved by the University of Arizona Institutional Animal Care and Use Committee. Six-week-old C57BL/6J male mice (Jackson Laboratory, Bar Harbor, ME) were infected as reported previously.[26] Briefly, streptomycin-treated mice (5 g/L streptomycin in drinking water ad libitum for 24 hours, followed by sterile water for 24 hours), were gavaged with 150 μL sterile PBS (control, uninfected), or 2×10^8 bacteria suspended in 150 μL sterile PBS, and monitored for up to 4 days after infection.

Attachment Assays

To assess EPEC attachment to the intestinal mucosa, WT- or SE874-infected C57BL/6J mice were euthanized on days 3 and 4 after infection (4 animals per condition). Segments of the cecum and proximal colon were isolated, cleaned, weighed, homogenized, serially diluted in PBS, and bacteria were enumerated on MacConkey agar containing 100 μg/mL nalidixic acid.

Fecal Shedding of EPEC

Mouse stool samples were collected daily for 4 days after infection, and weighed, homogenized in PBS, serially diluted, and bacteria were enumerated on MacConkey agar containing 100 μg/mL nalidixic acid. No colonies were recovered from the stool of uninfected animals, consistent with media selectivity for EPEC.

Immunofluorescence Microscopy

Cultured monolayers were grown on poly-L-lysine–coated coverslips. For mouse intestinal tissues, samples were frozen in OCT embedding medium (Tissue-Tek; Sakura Finetek, Torrance, CA) and stored at -80°C. Cultured monolayers and OCT-mounted tissue samples cut at 4-micron thickness were fixed in a 1:1 mixture of methanol and acetone for 20 minutes at -20°C, air-dried, rehydrated in PBS for 5 minutes, permeabilized with 0.2% Triton X-100 (Sigma-Aldrich, St. Louis, MO) in PBS for 15 minutes, and blocked with 5% IgG-free bovine serum albumin (BSA) in PBS for 1 hour. Primary antibodies used for cultured cells were 1:40 dilution of mouse anti-DSG2 and 1:1000 dilution of rabbit anti–lysosomal-associated membrane protein 1 (Abcam); mouse tissues were probed with 1:40 dilution of rabbit anti-DSG2 (Sigma Aldrich). Samples were incubated with primary antisera overnight at 4°C, and then washed 3 times with 1% IgG-free BSA in PBS. Secondary antibodies (Alexa 488–conjugated goat anti-mouse IgG, Alexa Fluor 555–conjugated anti-rabbit IgG, or Alexa 488 goat anti-rabbit IgG antisera; Thermo Fisher Scientific) were added at 8 μg/mL in 5% IgG-free BSA for 1 hour. Samples were washed with PBS, stained with 4,6-diamidino-2-phenylindole, and mounted in ProLong Diamond Antifade reagent (Thermo Fisher Scientific). Images were captured on a DeltaVision Elite Deconvolution Microscope (GE Healthcare, Pittsburgh, PA) using an Olympus 60×/1.42 objective with 1.59× auxiliary magnification or an Olympus 100×/1.4 objective (immersion oil refractive index, n = 1.516) (Sigma-Aldrich).

Transmission Electron Microscopy

Polarized IECs grown on 0.33-cm^2 collagen-coated Transwells (Thermo Fisher Scientific) were apically infected with EPEC strains cultured in DMEM. IECs and tissue samples were fixed in Karnovsky's Fixative (Electron Microscopy Sciences, Hatfield, PA) overnight at 4°C, neutralized with 125 mmol/L glycine in PBS, postfixed in 1% osmium tetroxide, and sequentially dehydrated with 15%, 30%, 50%, 70%, 90%, and 100% ethanol. Samples then were infiltrated with Spurr's Resin (Electron

Microscopy Sciences). Ultrathin sections were contrasted with 2% uranyl acetate, followed by Reynold's lead citrate, and visualized with an FEI Tecnai Spirit transmission electron microscope (FEI, Hillsboro, OR).

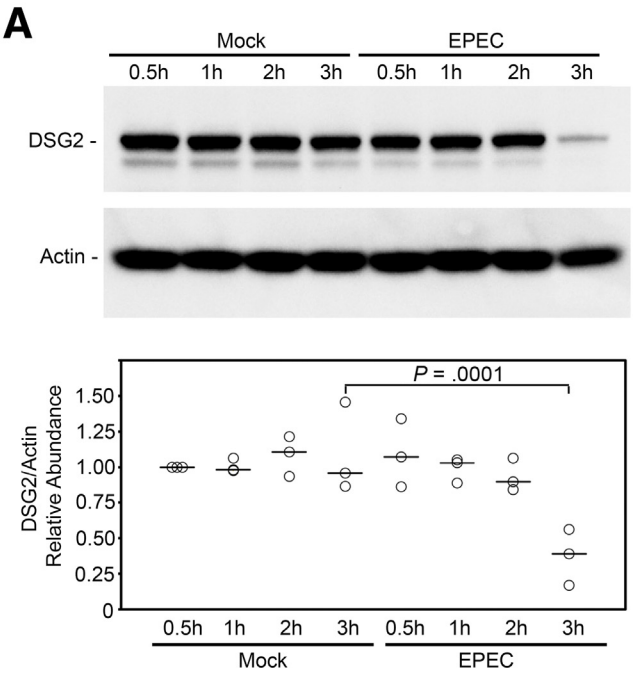

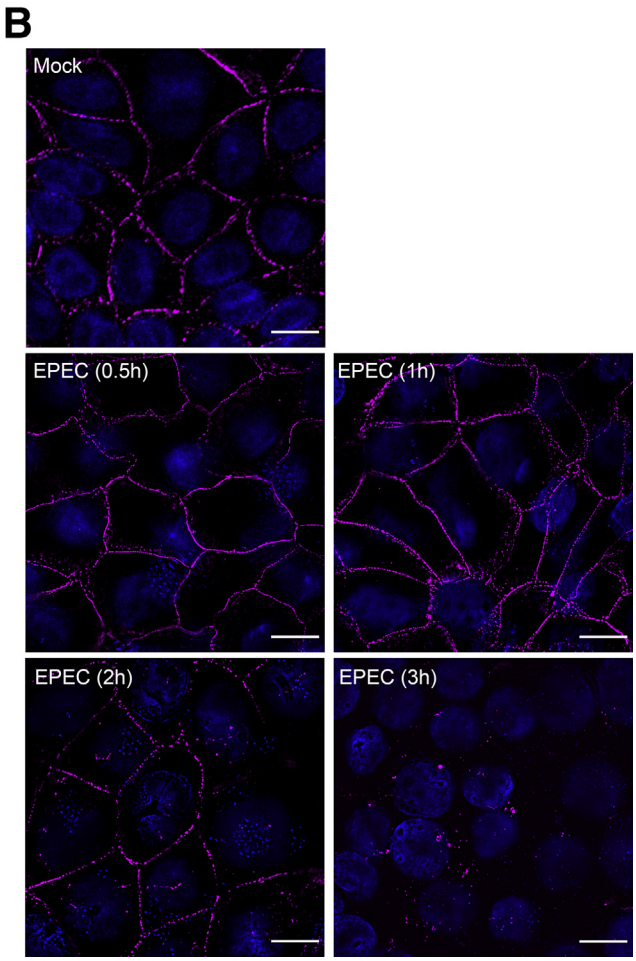

Statistical Analyses

Significant changes for all pairwise sample comparisons in experiments involving quantitation were assessed by analysis of variance with Bonferroni post hoc test.

All authors had access to the study data and have reviewed and approved the final manuscript.

Results

EspH Mediates Desmoglein-2 Loss in EPEC-Infected Epithelial Cells

To explore the molecular basis for the cell–cell separation previously seen in EPEC-infected patient tissues,[19] infected IEC extracts were immunoblotted for the transmembrane, spot-weld protein DSG2, the only desmoglein isoform present in the intestine. We observed substantial DSG2 loss at 3 hours after EPEC infection, but not in mock-treated cells (Figure 1*A*). Immunofluorescence of mock-treated cells, and cells infected with WT EPEC for up to 1 hour, showed the typical junctional localization of DSG2 noted previously.[27] At 2 hours after infection, there was evidence of DSG2 displacement from the cell junctions, and internalization of this protein into the cytosol (Figure 1*B*); by 3 hours, DSG2 was substantially depleted from infected cells, mirroring the immunoblot results.

In contrast to WT EPEC, an isogenic T3SS-deficient strain (Δ*espA*) failed to deplete DSG2 (Figure 2*A*), suggesting a role for 1 or more secreted effectors in the process. To identify the effector proteins involved, we assessed DSG2 abundance in IECs infected with isogenic EPEC mutants lacking specific effector molecules. EPEC Δ*map*, Δ*tir*, Δ*espG*, Δ*espF*, and Δ*espZ* caused DSG2 loss similar to the WT strain, ruling out a role for the corresponding effectors in DSG2 down-regulation (not shown). A strain lacking EspH (SE874), however, failed to deplete DSG2, and this defect was reversed by *espH* complementation (SE874/C) (Figure 2*B*). The major heterotypic partner of DSG2, DSC2, also was depleted in EPEC-infected IECs in an EspH-dependent manner (Figure 2*C*). Although DSC2 is the primary isoform expressed in the normal intestine, other desmocollin

Figure 1. EPEC induces desmoglein-2 loss. $C2_{BBe}$ monolayers were mock-treated, or infected with EPEC at a multiplicity of infection of 100 for 0.5, 1, 2, and 3 hours. (*A*) Whole-cell extracts of mock-treated or EPEC-infected $C2_{BBe}$ were immunoblotted for DSG2 and actin loading control. Scatter plot shows the densitometry analysis of the abundance of DSG2/actin of each sample compared with mock 0.5 h (3 independent experiments). The median values are indicated by *horizontal lines*. *P* values for the DSG2/actin ratio of EPEC 3 hours vs mock 3 hours were computed using analysis of variance with the Bonferroni post hoc test. (*B*) Immunofluorescence staining of DSG2 (magenta) in mock-treated or EPEC-infected $C2_{BBe}$ imaged with the DeltaVision Elite Deconvolution Microscope equipped with an Olympus 100×/1.40 oil objective and using immersion oil (n = 1.516). 4,6-Diamidino-2-phenylindole (blue) was used to stain DNA. *Scale bar*: 10 μm. Blots and images are representative of 3 independent experiments. For immunofluorescence staining, at least 6 fields per sample were captured in each experiment.

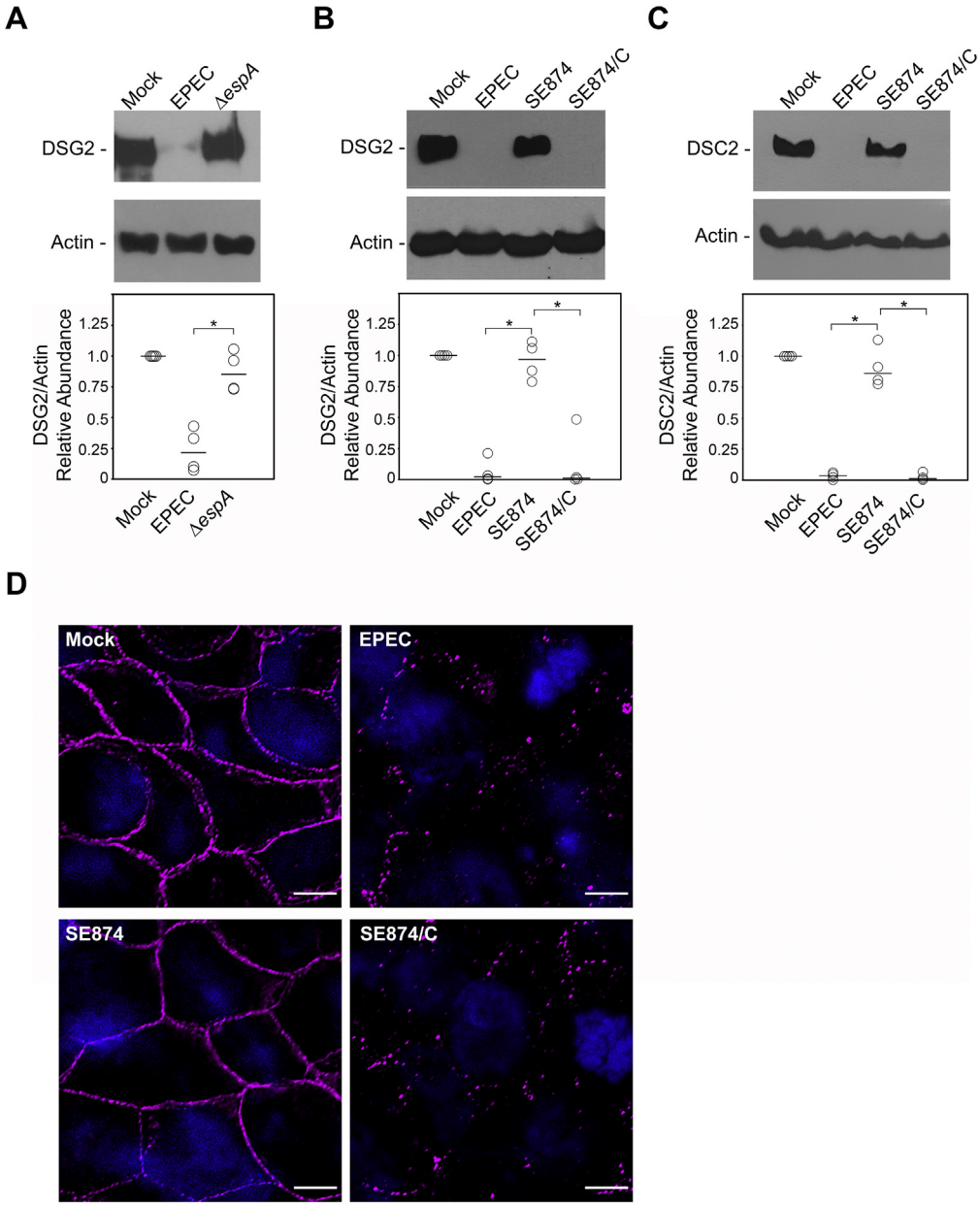

Figure 2. EPEC EspH induces desmoglein-2 redistribution and loss. (*A–C*) Whole-cell extracts of $C2_{BBe}$ mock-treated, or infected with EPEC, (*A*) the T3SS mutant Δ*espA*, or (*B* and *C*) *espH* mutant SE874 and corresponding complement SE874/C were immunoblotted for (*A* and *B*) DSG2 or (*C*) DSC2, and (*A–C*) actin loading control. Blots shown are representative of 4 independent experiments. Scatter plot shows densitometry analysis of the abundance of DSG2 or DSC2 relative to actin, respectively, for each sample compared with mock. *Horizontal lines* represent median values. *$P = .0001$ for the DSG2/actin ratio of specific sample comparisons calculated using analysis of variance with the Bonferroni post hoc test. (*D*) Immunofluorescence staining of DSG2 (magenta) in mock-, EPEC-, SE874-, and SE874/C-infected $C2_{BBe}$ cells imaged using the DeltaVision Elite Deconvolution Microscope equipped with an Olympus 100×/1.40 oil objective and immersion oil (n = 1.516). 4,6-Diamidino-2-phenylindole (blue) was used to stain DNA. *Scale bar*: 6 μm. Images are representative of at least 3 independent experiments. All immunofluorescence images are representative of >6 fields per sample captured for each independent experiment.

isoforms have been observed in disease states.[28] Therefore, all further studies focus on DSG2, with DSC2 included as a validation control where appropriate. In contrast to WT-infected cells, junctional DSG2 staining was maintained in mock-treated and SE874-infected cells (Figure 2*D*); complementation (SE874/C) restored the ability of the *espH* mutant to displace DSG2 from the junctions and cause its depletion.

Previous studies have shown the perturbation of TJs in EPEC-infected intestinal epithelial cells, notably the displacement of occludin and zonula occludens 1 from the TJ regions.[13–17] In some images of intestinal epithelia from

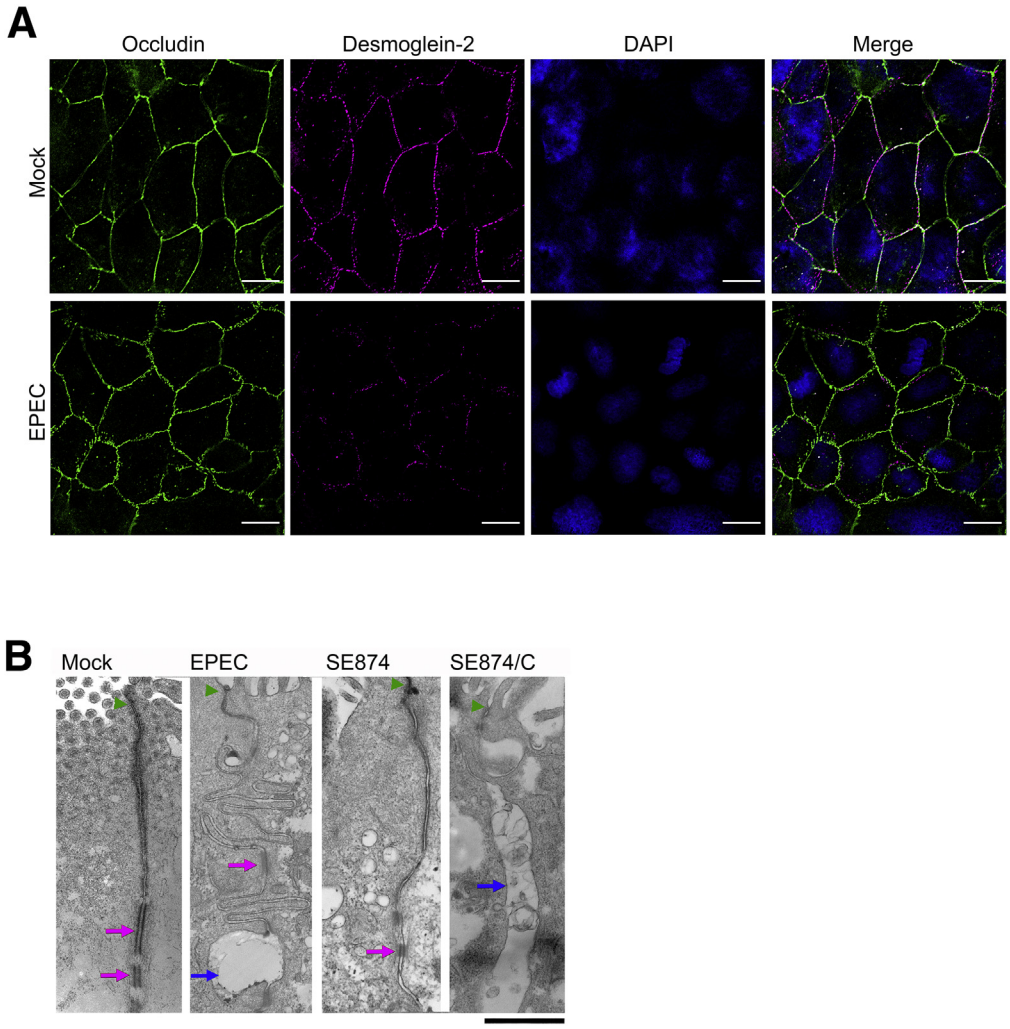

Figure 3. Desmoglein-2 perturbation precedes tight junction disruption in EPEC-infected cells. (*A* and *B*) $C2_{BBe}$ cells were infected with EPEC at a multiplicity of infection of 100 for 3 hours. (*A*) Cells were stained for desmoglein-2 (magenta), tight junction protein occludin (green), and 4,6-diamidino-2-phenylindole (DAPI; blue). All images were imaged using the DeltaVision Elite Deconvolution Microscope equipped with an Olympus 60×/1.42 oil objective and 1.59 auxiliary magnification and using immersion oil (n = 1.516). *Scale bar*: 6 μm. (*B*) EPEC EspH perturbs desmosomes. Transmission electron micrographs of mock-treated (*left-most panel*) or infected IECs showing desmosomes (*magenta arrows*) and areas of unzipping and separation of lateral membranes (*blue arrows*). *Green arrowheads* point to TJs. *Scale bar*: 500 nm. All images are representative of at >6 fields captured per sample from 3 independent experiments.

biopsy specimens of EPEC-infected children, however, TJs appeared intact in regions where basolateral unzipping was evident. We therefore used immunofluorescence to assess the temporal relationship between TJ and desmosomal disruptions in EPEC-infected epithelial cells. At 3 hours after infection, occludin staining was restricted primarily to the junctions of infected epithelial cells compared with mock-treated cells (Figure 3*A*). In contrast, DSG2 is substantially internalized and lost by this time point, suggesting that desmosomal alterations precede TJ disruption.

Because EPEC depletes DSG2 and DSC2, we assessed desmosomal integrity in infected cells via transmission electron microscopy. Densely staining desmosomes tracked along the lateral walls of mock-treated IECs, as well as cells infected with SE874 (Figure 3*B*). In contrast, WT EPEC- or SE874/C-infected cells had reduced desmosomal staining, areas of unzipping, and junctional separation. Notably, despite separation of the lateral membranes, TJs appeared intact, further indicating that desmosomal perturbations likely precede EPEC-induced TJ disruption. Collectively, these data suggest that EspH induces DSG2 displacement and loss from cell junctions, leading to desmosomal perturbations and loss of cell–cell contacts.

EPEC EspH Compromises Cell–Cell Adhesion and Epithelial Barrier Function

Because desmosomes are critical scaffolds between the lateral membranes of epithelial cells, we assessed the impact of EPEC-induced DSG2 loss on cell junction strength. Dispase-treated mock-infected and commensal *E coli*–infected cells, as well as Δ*espA*-infected and SE874-infected cells, were displaced from the plastic substratum, but remained as intact sheets (Figure 4*A*). In contrast, and consistent with EspH-dependent DSG2 loss, EPEC-infected and SE874/C-infected monolayers disintegrated into small fragments.

To determine if DSG2 loss impacted barrier function, we monitored infection-mediated TER changes in polarized $C2_{BBe}$ monolayers. WT EPEC induced a progressive decrease in TER relative to mock-treated epithelial cells (Figure 4*B*). Lack of EspH (SE874) markedly impaired the ability to decrease TER, while complementation (SE874/C) restored

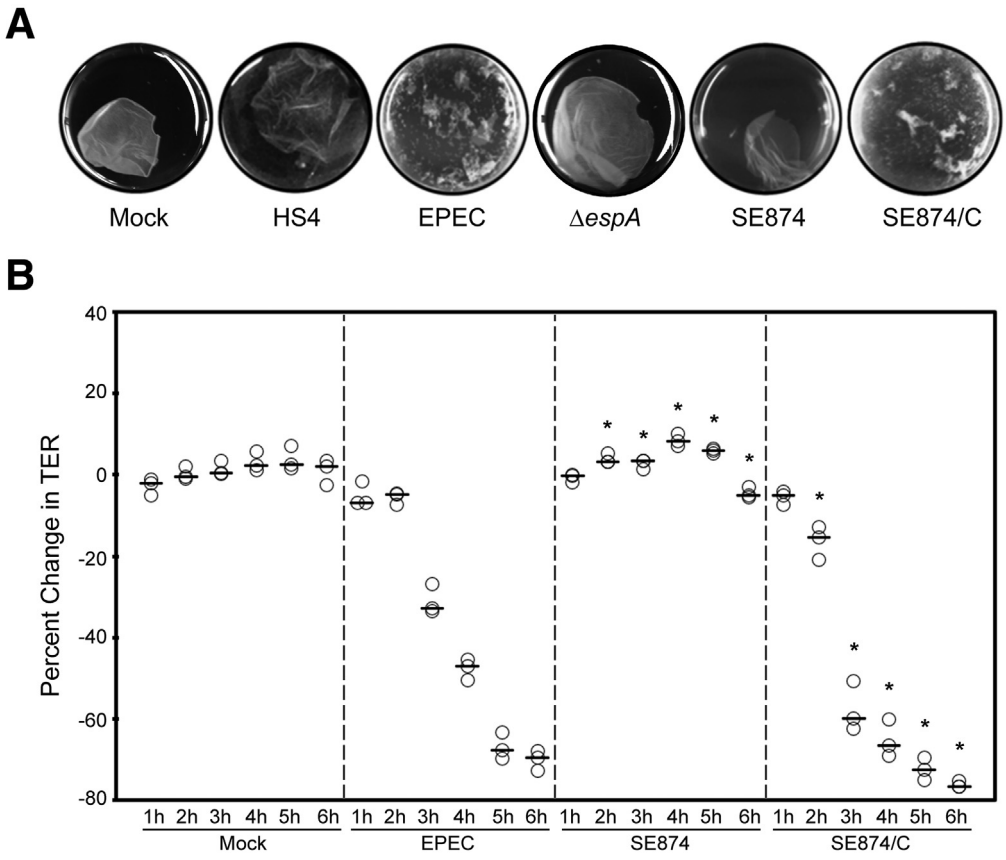

Figure 4. EspH weakens junctional integrity and disrupts barrier function of infected host epithelial monolayers. (*A*) Images showing $C2_{BBe}$ monolayer integrity after mock treatment, or infection with commensal *E coli* HS4, EPEC WT, Δ*espA*, SE874, and SE874/C, respectively, followed by dispase treatment and agitation. Images are representative of 3 independent experiments. (*B*) TER assays to measure barrier integrity in mock-, EPEC-, SE874-, or SE874/C-infected cells. Cells were infected at an initial multiplicity of infection of 100. **P* = .0001 for EPEC or SE874/C compared with SE874 for time points indicated. Data are representative of 3 independent TER assays with at least 3 sample replicates per condition.

the phenotype. Collectively, this suggests that EspH-induced DSG2 loss and desmosomal perturbations compromise epithelial monolayer integrity, leading to loss of epithelial barrier function.

EspH-Dependent DSG2 Redistribution and Loss Correlates With RhoA Inhibition

EspH (~168 amino acids) is unique to A/E pathogens, and does not show significant sequence similarity to other proteins. EspH interaction with Rho GEFs Dbl homology-plecstrin homology domains inhibits Rho GTPase activation, and perturbs the actin cytoskeletion.[29] However, the specific EspH residues involved in these processes remain undefined. To identify EspH domains involved in Rho GTPase inhibition, and in DSG2 relocalization, we generated a panel of alanine-scan mutants. The parent plasmid (encoding WT EspH) and mutant derivatives were used to complement the *espH*-deficient SE874 strain. Transfected $C2_{BBe}$ cells expressing p115-RhoGEF were infected with this panel of strains, and the extracts were assessed for EspH-p115 RhoGEF interactions. Co-immunoprecipitation studies confirmed interaction of EspH with p115-RhoGEF (Figure 5*A*); in contrast, 2 alanine-scan mutants, M14 and M16, with replacements of amino acids 88–92 and 98–102, respectively, failed to pull down p115-RhoGEF. The lesions in M14 and M16 did not compromise EspH secretion via the T3SS (Figure 5*A*).

The corresponding mutants were assessed for their ability to inhibit Rho GTPase activty. WT EPEC, but not SE874, inhibited RhoA activity in IECs (Figure 5*B*). Complementation of SE874 (SE874/C [=SE874/pJLR1] or SE874/pJLR4 [His-tagged EspH]) restored the ability to inhibit RhoA. In contrast, the RhoGEF interaction-defective mutants M14 and M16 failed to complement SE874 for RhoA inhibition (Figure 5*B*). Unlike WT *espH*-complemented SE874, M14- and M16-complemented SE874 also failed to induce the loss of DSG2, or its major heterotypic partner DSC2 (Figure 5*C*). Finally, M14 and M16 failed to complement SE874 for monolayer fragmentation, as assessed in the dispase assay (Figure 5*D*). Host-cell adherence of all strains was comparable with WT EPEC (not shown). These data support a model whereby EPEC EspH-mediated Rho GTPase inhibition promotes internalization and loss of the desmosomal proteins DSG2 and DSC2, causes the separation of the lateral membranes of adjacent cells, and compromises cell–cell adhesion and barrier function.

Mechanism of EspH-Mediated DSG2 Loss in Infected Cells

EspH competitively binds to RhoGEFs and inhibits Rho GTPase activation.[29] Although Rho GTPases were implicated in desmosomal protein anchoring to IFs in keratinocytes,[30] their contributions to desmosomal integrity in IECs has not been investigated. We therefore explored if Rho

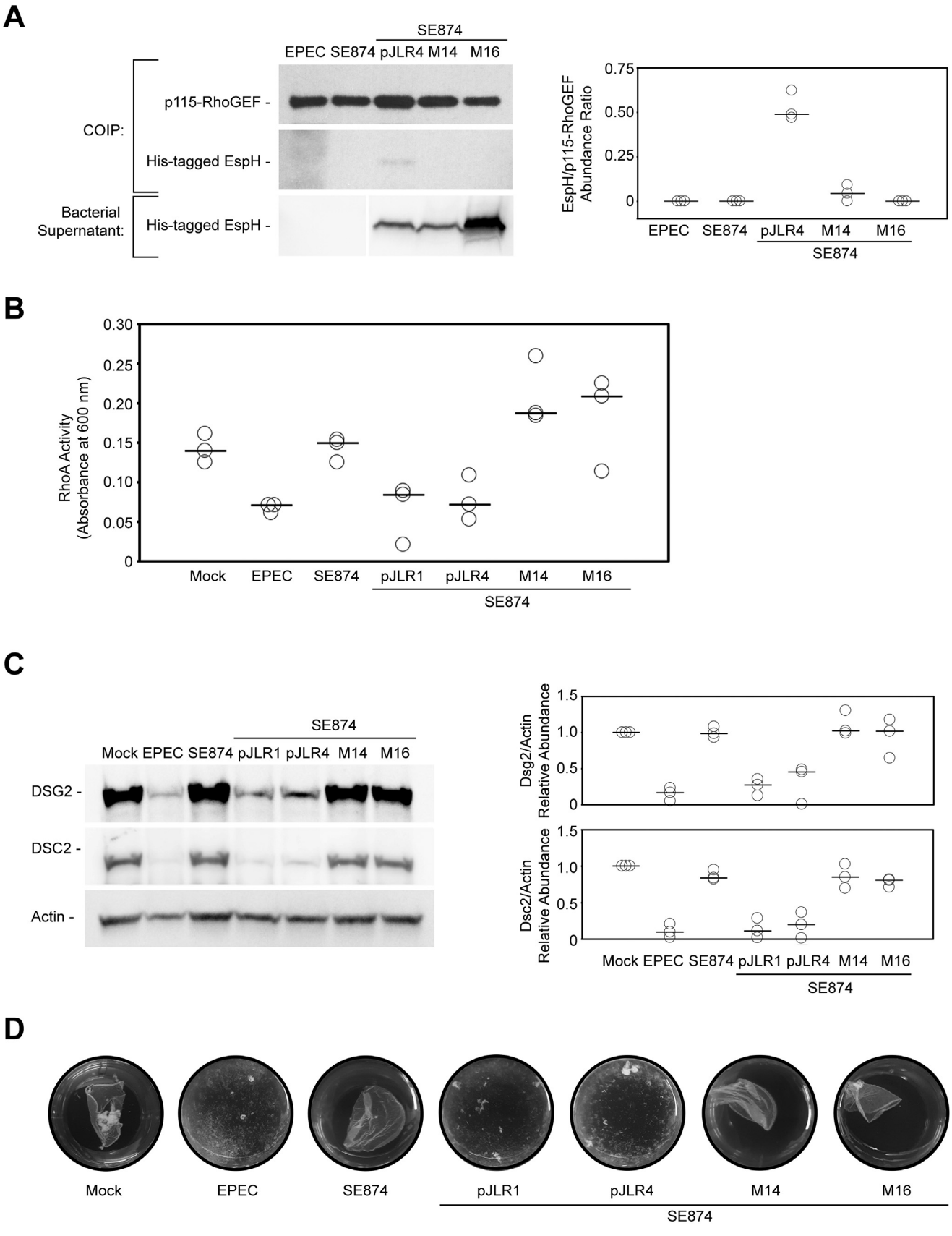
A
SE874
EPEC SE874 pJLR4 M14 M16
COIP:
p115-RhoGEF -
His-tagged EspH -
Bacterial Supernatant:
His-tagged EspH -
EspH/p115-RhoGEF Abundance Ratio
0.75
0.50
0.25
0
EPEC SE874 pJLR4 M14 M16
SE874
B
RhoA Activity (Absorbance at 600 nm)
0.30
0.25
0.20
0.15
0.10
0.05
0
Mock EPEC SE874 pJLR1 pJLR4 M14 M16
SE874
C
SE874
Mock EPEC SE874 pJLR1 pJLR4 M14 M16
DSG2 -
DSC2 -
Actin -
Dsg2/Actin Relative Abundance
Dsc2/Actin Relative Abundance
1.5
1.0
0.5
0
Mock EPEC SE874 pJLR1 pJLR4 M14 M16
SE874
D
Mock
EPEC
SE874
pJLR1
pJLR4
M14
M16
SE874

activator II CN03 could rescue RhoA activation and restore DSG2 levels downstream of the EspH-RhoGEF block. CN03 is based on the catalytic domain of cytotoxic necrotizing factor 1, which irreversibly deamidates Gln63 of RhoA and locks it in the active confirmation.[31,32] Although EPEC infection depleted DSG2 in infected cells, CN03 treatment restored DSG2 abundance (Figure 6*A*) and its localization (Figure 6*B*). CN03 alone did not have discernable impacts on DSG2 abundance or localization in mock-treated cells (Figure 6*A* and *B*). This further supports the contention that EspH induces DSG2 loss by inhibiting Rho GTPases.

To our knowledge, there is no known pathway linking Rho GTPases to DSG2 stabilization at cell junctions. Because Rho GTPase activation can stimulate actin polymerization, we considered a role for cytoskeletal modulation in EPEC-induced DSG2 down-regulation. The actin cytoskeleton plays a role in maintaining keratin IFs, and facilitates IF anchorage to desmosomes via the cytolinker desmoplakin.[33,34] Keratin IF precursors nucleate at desmosomes, and then translocate continuously toward the nucleus until they integrate end-on into the peripheral IF network.[35] Importantly, this inward-directed transport of keratin IF precursors depends on actin retrograde flow.[36] We therefore hypothesized that EspH-mediated Rho inactivation and consequent actin destabilization impairs the normal actin-dependent transport of keratin IFs, ultimately disrupting DSG2 and desmosome -anchoring at the junctions. To test this hypothesis, we infected IECs with EPEC strains and visualized IFs (via cytokeratin 8/18 staining) and DSG2. Consistent with our hypothesis, keratin staining was disrupted, or absent, in IECs infected with WT EPEC and SE874/C (Figure 6*C*); in several cells, the staining was suggestive of IF collapse away from the cell periphery, and toward the nucleus. Keratin staining remained intact, and comparable with mock-treated cells, in SE874-infected IECs (Figure 6*C*). This suggests that EspH impedes the inward-directed transport of new and maturing keratin IFs. Consistent with a role for cytoskeletal perturbation in this process, the actin-stabilizing drug jasplakinolide preserved IF integrity and DSG2 membrane localization in EPEC- and SE874/C-infected cells (Figure 6*C*). In the absence of infection, jasplakinolide did not impact DSG2 localization or abundance. Together, these data suggest that EspH-dependent Rho GTPase inactivation leads to actin depolymerization; this, in turn, perturbs IF stability and, ultimately, leads to destabilization of desmosomes and DSG2 down-regulation.

DSG2 Is Internalized and Degraded in the Lysosomes of EPEC-Infected Cells

Destabilized desmosomes can split into half-desmosomes and be internalized; in keratinocytes, desmogleins are degraded via the lysosomal or proteasomal pathways.[37] To assess DSG2 fate in EPEC-infected IECs, we determined the effects of the lysosomal inhibitor bafilomycin A1 and the proteasomal inhibitor MG132. Bafilomycin A1, but not the vehicle dimethyl sulfoxide, prevented EPEC-induced DSG2 loss (Figure 7*A*). MG132 had no apparent impact on infection-induced DSG2 displacement from the cell junctions to the cytosol (Figure 7*B*), but partially protected against DSG2 loss (Figure 7*A*). In contrast, lysosomal inhibition protected against EPEC-induced DSG2 loss (Figure 7*A*); moreover, DSG2 was internalized, and co-localized with lysosomal-associated membrane protein 1 in bafilomycin-treated, EPEC-infected IECs (Figure 7*B*). Taken together, these results suggest that EPEC EspH promotes junctional instability of DSG2, leading to its internalization and subsequent degradation primarily within lysosomes.

We explored 2 alternate pathways for direct DSG2 cleavage in EPEC-infected cells. EspH activates caspase-3, a cysteine–aspartic acid protease involved in programmed cell death.[38] EPEC also activates calcium-dependent

Figure 5. (***See previous page***). **EspH inhibition of RhoA correlates with DSG2 loss and weakening of cell–cell interactions in EPEC-infected monolayers.** (*A*) Transfected $C2_{BBe}$ cells expressing Flag-tagged p115-RhoGEF were infected with EPEC, SE874, or SE874 complemented with pJLR4 (WT, His-tagged) or alanine scan mutants M14 (88AAAAA92) or M16 (98AAAAA102). Flag-tagged p115-RhoGEF were immunoprecipitated from whole-cell extracts using anti-Flag antibody. Immunoprecipitated samples were blotted for p115-RhoGEF and His-tagged EspH. Blots shown are representative of 3 independent experiments. Densitometry analysis shows abundance of co-immunoprecipitated His-tagged EspH relative to p115-RhoGEF. *Horizontal line* represents median. Corresponding bacterial supernatants were concentrated and blotted for His-tagged EspH. Image is of a single gel with irrelevant lanes removed. *P* values for complemented strains, relative to SE874, are .0001 (pJLR4), .222 (M14), and 1.000 (M16), respectively. (*B*) RhoA activity in lysophosphatidic acid–treated $C2_{BBe}$ cells infected with EPEC, SE874, SE874/C, or SE874 complemented with pJLR4 (his-tagged EspH), M14, or M16 (alanine-scan mutants). Images are representative of 2 independent RhoA activity assays with 3 sample replicates per condition. *P* values are .0192 (mock vs EPEC) and .9721 (mock vs SE874); for the complemented strains, relative to SE874, *P* values are .0145 (pJLR1), .0364 (pJLR4), .0303 (M14), and .1797 (M16), respectively. (*C*) Extracts of mock-treated $C2_{BBe}$ cells, or $C2_{BBe}$ infected with the same strains as in panel *B* immunoblotted for DSG2 and DSC2 (*upper two panels*), and actin (loading control, *lower panel*). Scatter plot shows densitometry analysis of the abundance of DSG2/actin or DSC2/actin for each sample compared with mock. *Horizontal line* represents median. For DSG2/actin abundance ratios, $P = .0001$ for mock vs EPEC and mock vs SE874. *P* for the complemented strains, relative to SE874, are .0001 (pJLR1), .0002 (pJLR4), .4506 (M14), and .7078 (M16), respectively. For DSC2/actin abundance ratios, $P = .0001$ for mock vs EPEC and mock vs SE874. *P* values for the complemented strains, relative to SE874, are .0001 (pJLR1), .0001 (pJLR4), .9030 (M14), and .3527 (M16), respectively. (*D*) Dispase assays using the same strains described in panel *B*, and visualization of cell junctional integrity after mechanical agitation. All images for immunoblot and dispase assay are representative of 3 independent experiments. All infections were performed at an initial multiplicity of infection of 100 for 3 hours. COIP, co-immunoprecipitation.

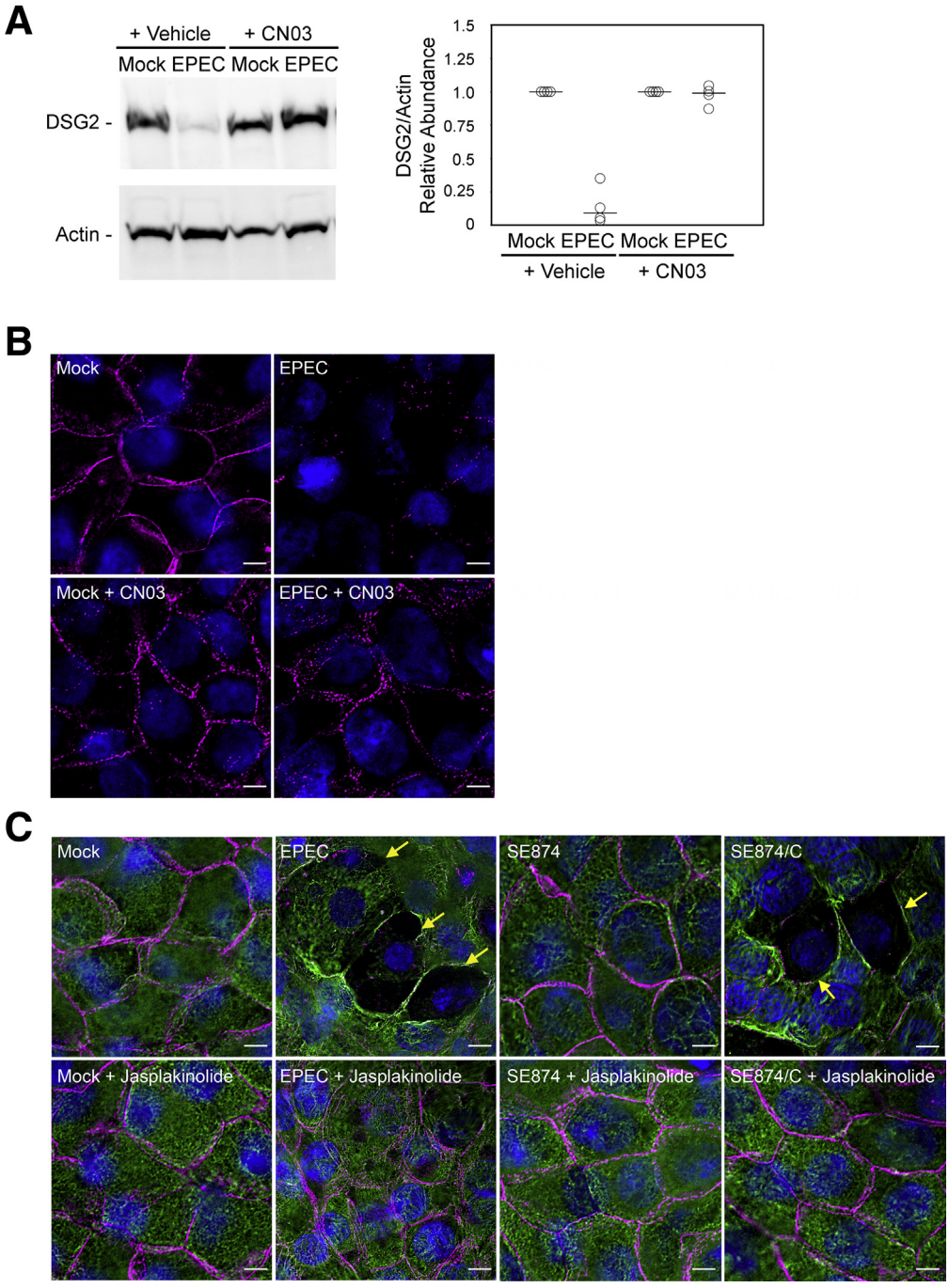

Figure 6. Rho GTPase activation, as well as actin stabilization, rescues EPEC-infected cells from DSG2 loss. (*A* and *B*) $C2_{BBe}$ cells were pretreated with H_2O vehicle control (*A*, lanes 1 and 2; *B*, upper row), or 300 ng/mL CN03 (*A*, lanes 3 and 4; *B*, bottom row) for 1 hour before, and continuing through, EPEC infection. Total proteins were extracted and analyzed for the abundance of (*A*) DSG2, or infected cells fixed and immunostained for (*B*) DSG2 (magenta) and 4,6-diamidino-2-phenylindole (DAPI; blue). (*A*) Scatter plot shows densitometry analysis of the abundance of DSG2/actin of EPEC-infected sample compared with corresponding mock. *Horizontal line* represents median. Immunoblots are representative of 4 independent experiments. $P = .0001$ (mock + vehicle vs EPEC + vehicle), .6657 (mock + CN03 vs EPEC + CN03), and .0001 (EPEC + vehicle vs EPEC + CN03). (*C*) $C2_{BBe}$ cells were pretreated with dimethyl sulfoxide vehicle control or 1 μmol/L jasplakinolide for 1 hour before, and continuing through, infection (mock, WT EPEC, SE874, or SE874/C), and fixed and immunostained for DSG2 (magenta), cytokeratin 8/18 [green], and DAPI [blue]. Infections were performed at an initial multiplicity of infection of 100 for 3 hours. *Arrows* mark IF retraction from cell membranes. All immunofluorescence images were captured using the DeltaVision Elite Deconvolution Microscope equipped with an Olympus 60×/1.42 oil objective and using immersion oil (n = 1.516), and are representative of >6 fields per sample from 3 independent experiments. *Scale bar*: 11 μm.

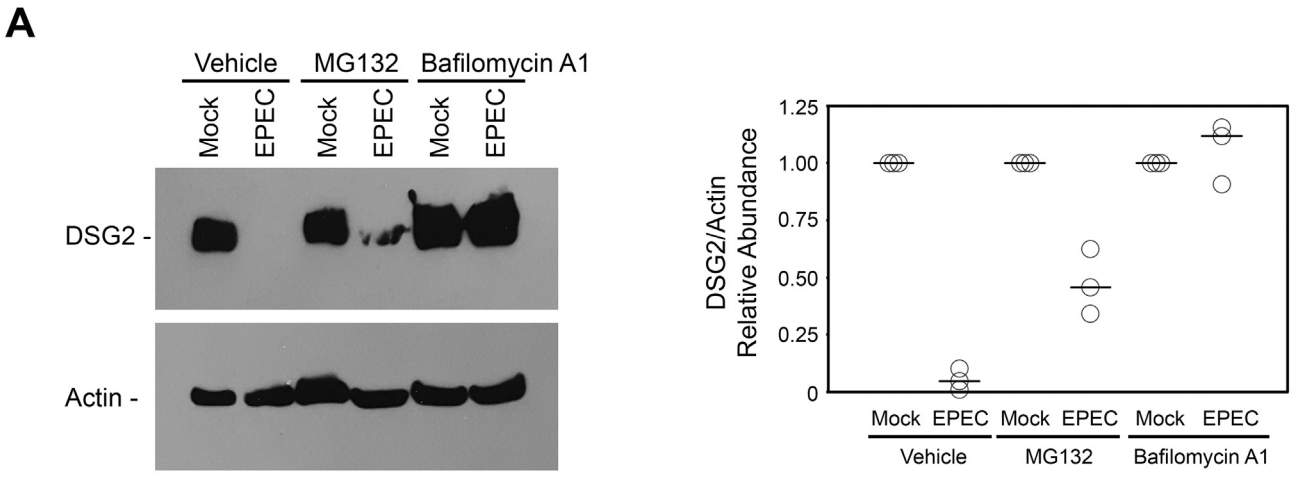

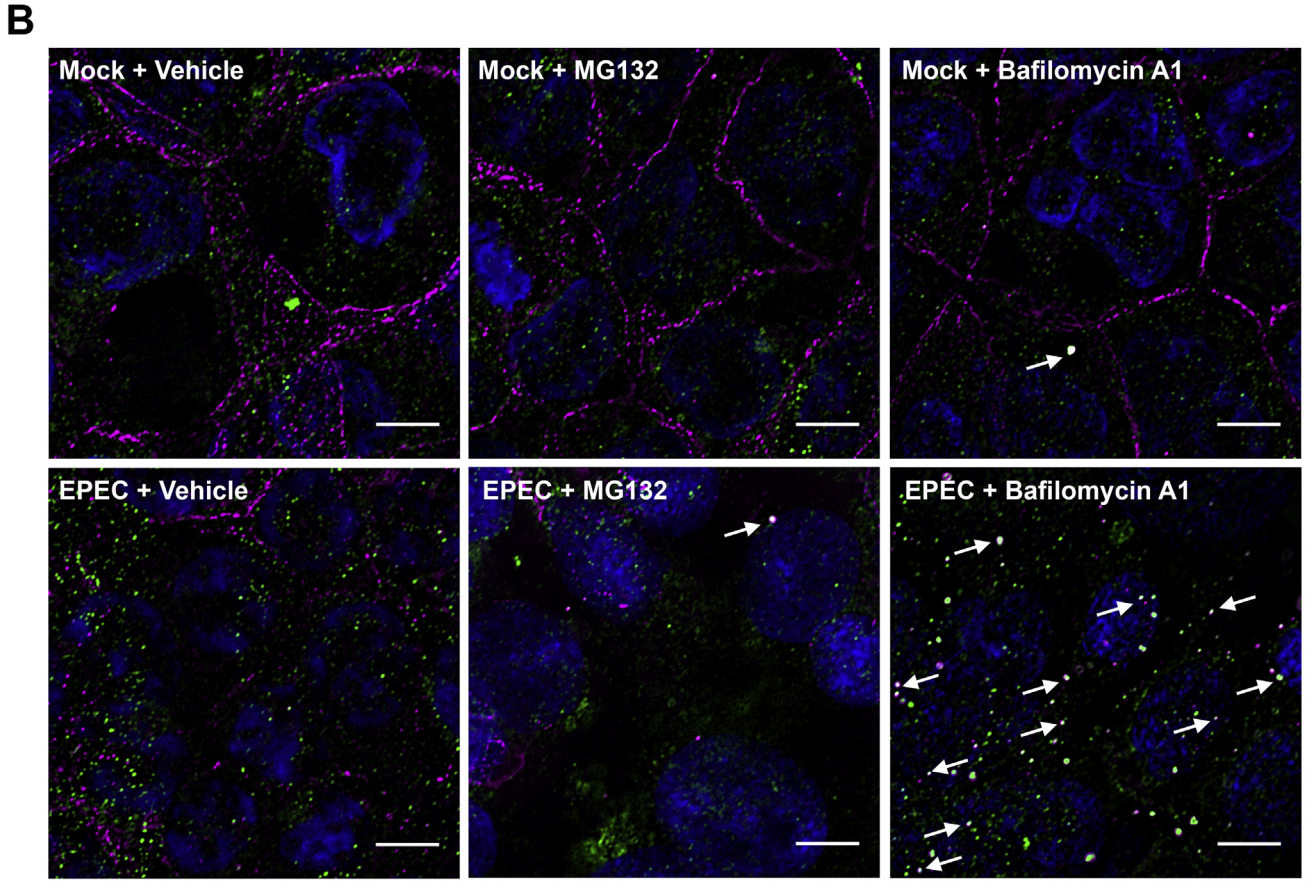

Figure 7. DSG2 is degraded in the lysosomes of EPEC-infected cells. $C2_{BBe}$ cells were pretreated with 250 nmol/L lysosomal inhibitor bafilomycin A1, 10 μmol/L proteasomal inhibitor MG132, or dimethyl sulfoxide vehicle control for 2 hours before infection with EPEC at a multiplicity of infection of 100 for 3 hours. Inhibitor concentrations were maintained throughout the course of infection. (*A*) Total protein extracts immunoblotted for DSG2 (or actin; loading control). Scatter plot shows densitometry analysis of the abundance of DSG2/actin of EPEC-infected sample compared with corresponding mock. *Horizontal line* represents median. Immunoblots are representative of 3 independent experiments. $P = .0001$ for EPEC + MG132 and EPEC + bafilomycin A1 compared with EPEC + vehicle, respectively. (*B*) Mock-treated and infected cells were fixed and immunostained for DSG2 (magenta), lysosomal-associated membrane protein 1 (LAMP1; green), and 4,6-diamidino-2-phenylindole (blue). *Arrows* point to co-localized DSG2 and LAMP1. All images were captured using the DeltaVision Elite Deconvolution Microscope equipped with an Olympus 100×/1.40 oil objective and using immersion oil (n = 1.516), and are representative of >6 fields per sample from 3 independent experiments.

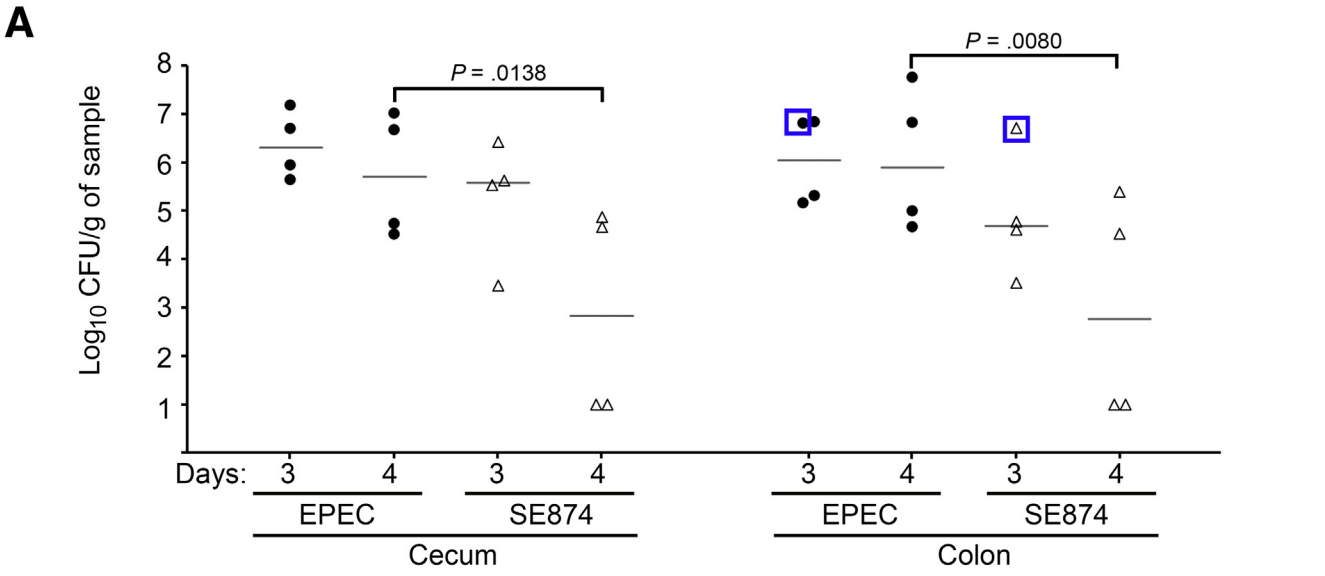
A
P = .0138
P = .0080
Log10 CFU/g of sample
8
7
6
5
4
3
2
1
Days: 3 4 3 4 3 4 3 4
EPEC
SE874
EPEC
SE874
Cecum
Colon

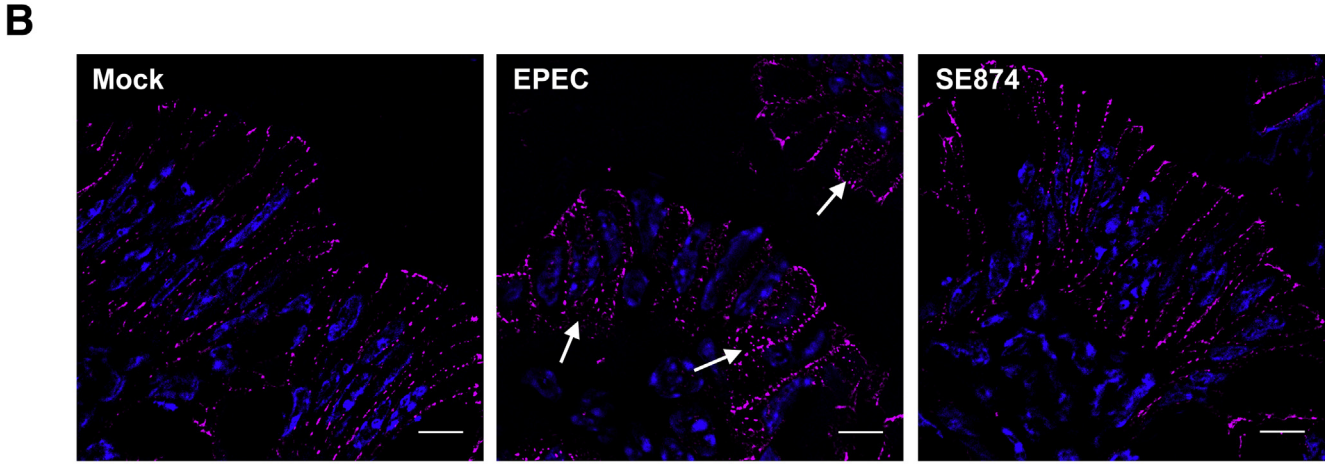
B
Mock
EPEC
SE874

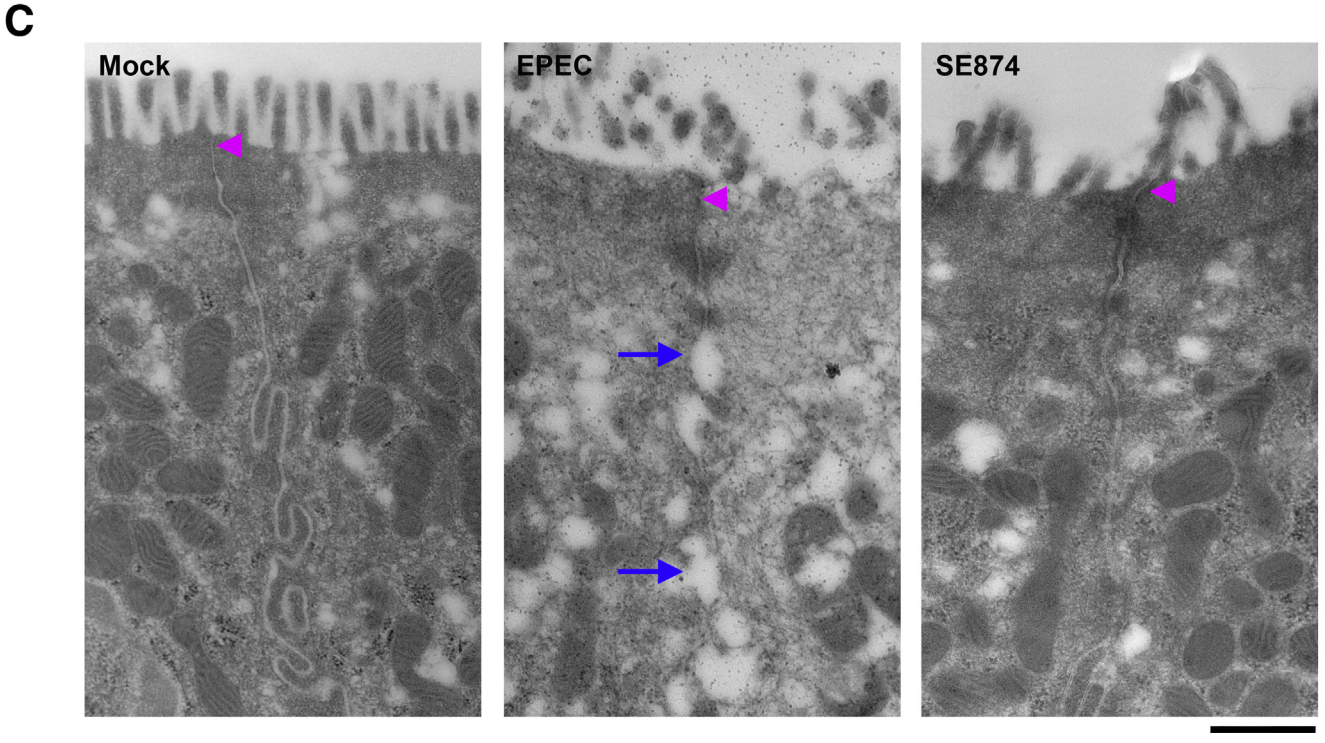
C
Mock
EPEC
SE874

nonlysosomal enzymes (calpains), although EspH has not been implicated in this pathway.[39] Because DSG2 is a known target of both caspases and calpains,[40] we assessed the effects of calpain inhibitor I and the pan-caspase inhibitor z-DEVD-fmk, respectively, on EPEC-induced DSG2 loss. Neither inhibitor impacted infection-induced DSG2 loss, indicating that caspases and calpains are not involved in this process (data not shown).

EspH Contributes to EPEC-Induced DSG2 Relocalization, and to Intestinal Colonization, in a Mouse Model of Infection

Finally, we assessed EPEC-induced DSG2 down-regulation and desmosomal perturbation in vivo using a mouse colonization model.[26,41] WT EPEC robustly colonized the mouse cecum and colon on days 3 and 4 after infection (Figure 8*A*). Although SE874 colonization of the cecum and colon were comparable with WT EPEC on day 3 after infection, its levels decreased at both sites by day 4 after infection (Figure 8*A*), suggesting a role for EspH in EPEC persistence in the mouse intestine. Both strains were shed at comparable levels on days 1–4 after infection (data not shown).

To investigate infection-induced DSG2 alterations in vivo, colonic tissues isolated on day 3 after infection, when WT EPEC and SE874 colonized at comparable levels, were subjected to immunofluorescence staining. In uninfected and SE874-infected mice, DSG2 was distributed uniformly along the colonic epithelial cell junctions (Figure 8*B*). In colon tissues of EPEC-infected mice, however, DSG2 was relocalized intracellularly into distinct puncta, consistent with our in vitro observations. Electron micrographs images of infected tissues showed separation of the lateral membranes of colonic epithelial cells in WT-infected mice, but not mock-treated or SE874-infected animals (Figure 8*C*). Notably, as previously seen in infant colon biopsy specimens,[19] and in vitro (Figure 4*B*), basolateral unzipping was evident in EPEC-infected mice even in areas where the TJs appeared unperturbed. Collectively, these data suggest that EspH mediates EPEC-induced DSG2 relocalization from intestinal epithelial junctions, its subsequent loss in the cytosol, and the consequent perturbation of cell–cell contacts. These changes likely contribute to EPEC colonization of the mouse intestine.

Discussion

As its primary virulence strategy, EPEC secretes effector proteins into IECs and alters their physiology.[12] We show that the RhoGEF-sequestering effector EspH inhibits RhoA activity and, correspondingly, induces the internalization and degradation of DSG2 and its major heterotypic partner, DSC2. This results in the loss of desmosomal contacts between adjacent cells, weakened cell–cell adhesion, and disruption of epithelial barrier function. The loss of desmosomal contacts could be a precursor to the cell rounding phenotype observed in EspH-expressing cells,[29,42] and the epithelial erosion previously seen in infected animal tissues.[43] Importantly, the mechanism outlined for EspH-dependent DSG2 depletion and desmosomal perturbation may provide a molecular basis for the basolateral junction widening observed in intestinal biopsy specimens from EPEC-infected infants.[19]

Rho GTPases were implicated in the maintenance of desmosomal integrity of keratinocytes and myocardial cells,[30,44–46] but their impact on desmosomes of the very different simple columnar intestinal epithelia is unknown. On the other hand, the effects of Rho GTPase signaling on intestinal epithelial TJs and adherens junctions have been characterized in some detail.[47] Our studies provide 2 lines of evidence for a key role for Rho GTPase signaling in maintaining IEC desmosomal junctions: EspH mutants that failed to inhibit RhoA also were unable to perturb desmosomes, and CN03-mediated Rho GTPase activation rescued EPEC-induced DSG2 loss.

EspH-induced Rho GTPase inhibition leads to actin cytoskeleton disruption[29]; our studies also implicate a role for EspH in perturbing the IF network. Our observations are consistent with a model whereby EspH-mediated Rho GTPase inactivation impedes the actin-dependent, inward-directed transport of cytokeratins from the periphery to the cell center, leading to IF retraction[35,36]; this, possibly in conjunction with displacement of the IF-desmosome linker, desmoplakin, induces DSG2 internalization into, and degradation in, lysosomes.[33,34] We previously described cytokeratin alterations in EPEC-infected cells partially mediated by EspF.[48] EspF therefore also may contribute to desmosomal perturbations. However, given the profound deficiency of cytokeratin and DSG2 perturbations in cells

Figure 8. (***See previous page***). **EspH contributes to EPEC persistence in the mouse gut, DSG2 redistribution, and disruption of mouse intestinal epithelial cell junctions.** C57BL/6J mice were mock-treated or infected with EPEC or SE874. (*A*) Colonization of the cecum and colon on days 3 and 4 after infection (N = 4 per sample group) were evaluated by plating on selective media. *Horizontal line* represents median. *P* values were computed using analysis of variance with the Bonferroni post hoc test. Colon tissues of mock-treated or day 3 postinfected mice (N = 4 per sample group) were used for (*B*) immunofluorescence staining and (*C*) transmission electron microscopy experiments. (*A*) *Blue boxes* correspond to representative tissue samples of infected animals shown in panels *B* and *C*. (*B*) Colon tissues of mock-treated, EPEC-infected or SE874-infected mice were stained for DSG2 (magenta) and 4,6-diamidino-2-phenylindole (blue). *Arrows* point to punctate cytoplasmic DSG2 staining. Images were captured using the DeltaVision Elite Deconvolution Microscope equipped with an Olympus 40×/1.35 oil objective and using immersion oil (n = 1.516). *Scale bar*: 17 μm. (*C*) Transmission electron micrographs of colon tissues of mock-treated (*left panel*), EPEC-infected (*middle panel*), or SE874-infected (*right panel*) showing tight junctions (*magenta arrowheads*) and areas of unzipping and separation of lateral membranes (*blue arrows*). *Scale bar*: 500 nm. All immunofluorescence and transmission electron microscopy images are representative of at least 6 fields captured per sample from the 3 sample groups (n = 4 per sample group). CFU, colony-forming unit.

infected with SE874 (which lacks EspH, but expresses EspF), EspF may have only an ancillary role in this process.

Desmosomal perturbations have been reported in the context of other intestinal infections, notably with *Entamoeba histolytica*, *Giardia duodenalis*, and *Campylobacter jejuni*.[49–51] *E histolytica* EhCP112 protease cleaves several desmosomal proteins, including DSG2, but the underlying mechanisms for *C jejuni*– and *G duodenalis*–mediated desmosomal perturbation are unknown. The current study is a mechanistic characterization of Rho-dependent intestinal epithelial desmosomal perturbation. By extension, other enteric pathogens that harbor Rho GTPase-inactivating virulence proteins, such as *Clostridium difficile* (toxins TcdA and TcdB),[52] *Vibrio cholerae* (MARTX toxin),[53] and *Yersinia* (YopE, YpkA, and YopT)[54] may also promote desmosome destabilization. Beyond a possible role in the etiology of infectious diseases, a robust decrease in DSG2 levels was observed in the mucosa of patients with Crohn's disease.[45] It is noteworthy that there was an increased abundance of specific pathogenic *E coli* strains in a subset of Crohn's disease patients; many of these strains disrupt epithelial barrier function, but their impacts on desmosomal junctions have not been explored.[55]

Our work now adds EspH to the list of EPEC effector proteins that perturb epithelial paracellular permeability.[56] The impact of EspH on epithelial barrier function is novel and noteworthy because it suggests a role for desmosomes beyond that of inert scaffolding. Consistent with this hypothesis, small interfering RNA–mediated DSG2 down-regulation in IECs alters epithelial barrier function.[45] Interestingly, a tandem peptide-mediated stabilization of junctional DSG2 linkages in Caco-2 cells ameliorated TNF-α–induced barrier disruption.[45] Electron micrographs images of EPEC-infected epithelial cells suggest that DSG2 depletion and separation of lateral cell surfaces precede complete dissociation of TJs. Our data, however, do not rule out the possibility of a direct impact of EspH-mediated Rho inhibition on TJs, independent of, and in addition to, the desmosomal alterations.

In contrast to our observations, Guttman et al[57] noted that desmoglein and desmocollin remain unchanged during EPEC infection in vitro. The differences in experimental conditions between the 2 studies is a likely explanation for this discrepancy. Whereas Guttman et al[57] used subconfluent Caco-2 cells, our studies used confluent $C2_{BBe}$ cells that reportedly have maximal cell-junctional DSG2 distribution and stable desmosomes.

Interestingly, Guttman et al[57] also did not detect desmoglein redistribution in colonic tissues of mice infected with *Citrobacter rodentium*. This may well represent a true distinction between EPEC and *C rodentium*. Unlike the prototype EPEC strain used in this study, *C rodentium* secretes EspM2 and EspT, which mimic GEF activity for RhoA and Rac1, respectively. These effectors were shown to mitigate some impacts of EspH-mediated Rho GTPase suppression.[29,58–60] Consistent with this, *C rodentium* mutants lacking *espH* were not impaired for virulence in mouse infection studies, although they fared poorer in competition experiments with WT *C rodentium*.[61] In contrast, EPEC mutants lacking *espH* initially colonized the mouse cecum and colon at levels comparable with the parent WT strain (3 days after infection) but were recovered at lower levels on day 4 after infection. EspH-induced barrier perturbations may enhance nutrient flux into the intestine, which, in turn, may facilitate EPEC expansion; alternatively, the concomitant activation of inflammatory responses may deplete commensal organisms and provide EPEC a competitive edge. In a previous study, enterohemorrhagic *E coli* mutants lacking *espH* also were shown to be impaired for virulence in a rabbit model of infection.[62]

A comprehensive understanding of the role of EspH, as well as Rho GTPase inhibition and desmosomal changes in A/E pathogen virulence, therefore, requires due consideration of the specific model systems, and an appreciation for the cooperative action of effector molecules. In summary, we identified a novel role for EPEC EspH in perturbing intestinal epithelial desmosomal junctions, which likely contributes to disease. Our delineation of the underlying pathway of desmosomal disruption, involving Rho GTPases and the actin cytoskeleton, has broader implications for both normal intestinal function and for various pathologic states.

References

1. Groschwitz KR, Hogan SP. Intestinal barrier function: molecular regulation and disease pathogenesis. J Allergy Clin Immunol 2009;124:3–20.
2. Giepmans BN, van Ijzendoorn SC. Epithelial cell-cell junctions and plasma membrane domains. Biochim Biophys Acta 2009;1788:820–831.
3. Anderson JM, Van Itallie CM. Tight junctions and the molecular basis for regulation of paracellular permeability. Am J Physiol 1995;269:G467–G475.
4. Niessen CM. Tight junctions/adherens junctions: basic structure and function. J Invest Dermatol 2007;127:2525–2532.
5. Nekrasova O, Green KJ. Desmosome assembly and dynamics. Trends Cell Biol 2013;23:537–546.
6. Holthöfer B, Windoffer R, Troyanovsky S, Leube RE. Structure and function of desmosomes. Int Rev Cytol 2007;264:65–163.
7. Shabih-e-Hassnain S, Trinnaman B, Martin S, Major S, Hutchinson J, Magee AI. Molecular interactions between desmosomal cadherins. Biochem J 2002;362:317–327.
8. Capaldo CT, Farkas AE, Nusrat A. Epithelial adhesive junctions. F1000Prime Rep 2014;6:1.
9. Barreau F, Hugot J. Intestinal barrier dysfunction triggered by invasive bacteria. Curr Opin Microbiol 2014;17:91–98.
10. Lanata CF, Fischer-Walker CL, Olascoaga AC, Torres CX, Aryee MJ, Black RE. Child Health Epidemiology Reference Group of the World Health Organization and UNICEF. Global causes of diarrheal disease mortality in children <5 years of age: a systematic review. PLoS One 2013;8:e72788.
11. Nataro JP, Kaper JB. Diarrheagenic *Escherichia coli*. Clin Microbiol Rev 1998;11:142–201.

12. Berkes J, Viswanathan VK, Savkovic SD, Hecht G. Intestinal epithelial responses to enteric pathogens: effects on the tight junction barrier, ion transport, and inflammation. Gut 2003;52:439–451.
13. McNamara BP, Koutsouris A, O'Connell CB, Nougayrede JP, Donnenberg MS, Hecht G. Translocated EspF protein from enteropathogenic *Escherichia coli* disrupts host intestinal barrier function. J Clin Invest 2001;107:621–629.
14. Garber JJ, Mallick EM, Scanlon KM, Turner JR, Donnenberg MS, Leong JM, Snapper SB. Attaching-and-effacing pathogens exploit junction regulatory activities of N-WASP and SNX9 to disrupt the intestinal barrier. Cell Mol Gastroenterol Hepatol 2017;5:273–288.
15. Tomson FL, Viswanathan VK, Kanack KJ, Kanteti RP, Straub KV, Menet M, Kaper JB, Hecht G. EPEC EspG disrupts microtubules and in conjunction with Orf3 enhances perturbation of tight junction barrier. Mol Microbiol 2005;2:447–464.
16. Dean P, Kenny B. Intestinal barrier dysfunction by enteropathogenic *Escherichia coli* is mediated by two effector molecules and a bacterial surface protein. Mol Microbiol 2004;54:665–675.
17. Thanabalasuriar A, Koutsouris A, Weflen A, Mimee M, Hecht G, Gruenheid S. The bacterial virulence factor NleA is required for the disruption of intestinal tight junctions by enteropathogenic *Escherichia coli*. Cell Microbiol 2010;12:31–41.
18. Malladi V, Shankar B, Williams PH, Balakrishnan A. Enteropathogenic *Escherichia coli* outer membrane proteins induce changes in cadherin junctions of Caco-2 cells through activation of PKCalpha. Microbes Infect 2004;6:38–50.
19. Rothbaum RJ, Partin JC, Saalfield K, McAdams AJ. An ultrastructural study of enteropathogenic *Escherichia coli* infection in human infants. Ultrastruct Pathol 1983; 4:291–304.
20. Peterson MD, Mooseker MS. Characterization of the enterocyte-like brush border cytoskeleton of the $C2_{BBe}$ clones of the human intestinal cell line, Caco-2. J Cell Sci 1992;102:581–600.
21. Roxas JL, Ryan K, Vedantam G, Viswanathan VK. Enteropathogenic *Escherichia coli* dynamically regulates EGFR signaling in intestinal epithelial cells. Am J Physiol Gastrointest Liver Physiol 2014;307:G374–G380.
22. Elliott SJ, Krejany EO, Mellies JL, Robins-Browne RM, Sasakawa C, Kaper JB. EspG, a novel type III system-secreted protein from enteropathogenic *Escherichia coli* with similarities to VirA of *Shigella flexneri*. Infect Immun 2001;69:4027–4033.
23. Penfold RJ, Pemberton JM. An improved suicide vector for construction of chromosomal insertion mutations in bacteria. Gene 1992;118:145–146.
24. Bromberg Y, Rost B. Comprehensive in silico mutagenesis highlights functionally important residues in proteins. Bioinformatics 2008;24:i207–i212.
25. Jiang K, Rankin CR, Nava P, Sumagin R, Kamekura R, Stowell SR, Feng M, Parkos CA, Nusrat A. Galectin-3 regulates desmoglein-2 and intestinal epithelial intercellular adhesion. J Biol Chem 2014;289:10510–10517.
26. Royan SV, Jones RM, Koutsouris A, Roxas JL, Falzari K, Weflen AW, Kim A, Bellmeyer A, Turner JR, Neish AS, Rhee KJ, Viswanathan VK, Hecht GA. Enteropathogenic *E. coli* non-LEE encoded effectors NleH1 and NleH2 attenuate NF-kappaB activation. Mol Microbiol 2010; 78:1232–1245.
27. Schlegel N, Meir M, Heupel WM, Holthofer B, Leube RE, Waschke J. Desmoglein 2-mediated adhesion is required for intestinal epithelial barrier integrity. Am J Physiol Gastrointest Liver Physiol 2010;298:G774–G783.
28. Khan K, Hardy R, Haq A, Ogunbiyi O, Morton D, Chidgey M. Desmocollin switching in colorectal cancer. Br J Cancer 2006;95:1367–1370.
29. Dong N, Liu L, Shao F. A bacterial effector targets host DH-PH domain RhoGEFs and antagonizes macrophage phagocytosis. EMBO J 2010;29:1363–1376.
30. Waschke J, Spindler V, Bruggeman P, Zillikens D, Schmidt G, Drenckhahn D. Inhibition of Rho A activity causes pemphigus skin blistering. J Cell Biol 2006; 175:721–727.
31. Schmidt G, Sehr P, Wilm M, Selzer J. Gln 63 of Rho is deamidated by *Escherichia coli* cytotoxic necrotizing factor-1. Nature 1997;387:725.
32. Lemichez E, Flatau G, Bruzzone M, Boquet P, Gauthier M. Molecular localization of the *Escherichia coli* cytotoxic necrotizing factor CNF1 cell-binding and catalytic domains. Mol Microbiol 1997;24:1061–1070.
33. Godsel LM, Hsieh SN, Amargo EV, Bass AE, Pascoe-McGillicuddy LT, Huen AC, Thorne ME, Gaudry CA, Park JK, Myung K, Goldman RD, Chew TL, Green KJ. Desmoplakin assembly dynamics in four dimensions: multiple phases differentially regulated by intermediate filaments and actin. J Cell Biol 2005;171:1045–1059.
34. Kouklis PD, Hutton E, Fuchs E. Making a connection: direct binding between keratin intermediate filaments and desmosomal proteins. J Cell Biol 1994; 127:1049–1060.
35. Windoffer R, Beil M, Magin TM, Leube RE. Cytoskeleton in motion: the dynamics of keratin intermediate filaments in epithelia. J Cell Biol 2011;194:669–678.
36. Kolsch A, Windoffer R, Leube RE. Actin-dependent dynamics of keratin filament precursors. Cell Motil Cytoskeleton 2009;66:976–985.
37. McHarg S, Hopkins G, Lim L, Garrod D. Down-regulation of desmosomes in cultured cells: the roles of PKC, microtubules and lysosomal/proteasomal degradation. PLoS One 2014;9:e108570.
38. Wong AR, Clements A, Raymond B, Crepin VF, Frankel G. The interplay between the *Escherichia coli* Rho guanine nucleotide exchange factor effectors and the mammalian RhoGEF inhibitor EspH. MBio 2012;3:1.
39. Serapio-Palacios A, Navarro-Garcia F. EspC, an autotransporter protein secreted by enteropathogenic *Escherichia coli*, causes apoptosis and necrosis through caspase and calpain activation, including direct procaspase-3 cleavage. MBio 2016;7:3.
40. Nava P, Laukoetter MG, Hopkins AM, Laur O, Gerner-Smidt K, Green KJ, Parkos CA, Nusrat A. Desmoglein-2: a novel regulator of apoptosis in the intestinal epithelium. Mol Biol Cell 2007;18:4565–4578.

41. Roxas JL, Koutsouris A, Bellmeyer A, Tesfay S, Royan S, Falzari K, Harris A, Cheng H, Rhee KJ, Hecht G. Enterohemorrhagic *E. coli* alters murine intestinal epithelial tight junction protein expression and barrier function in a Shiga toxin independent manner. Lab Invest 2010; 90:1152–1168.
42. Tu X, Nisan I, Yona C, Hanski E, Rosenshine I. EspH, a new cytoskeleton-modulating effector of enterohaemorrhagic and enteropathogenic *Escherichia coli*. Mol Microbiol 2003;47:595–606.
43. Al-Mamun A, Mily A, Sarker P, Tiash S, Navarro A, Akter M, Talukder KA, Islam MF, Agerberth B, Gudmundsson GH, Cravioto A, Raqib R. Treatment with phenylbutyrate in a pre-clinical trial reduces diarrhea due to enteropathogenic *Escherichia coli*: link to cathelicidin induction. Microbes Infect 2013;15:939–950.
44. Gliem M, Heupel WM, Spindler V, Harms GS, Waschke J. Actin reorganization contributes to loss of cell adhesion in pemphigus vulgaris. Am J Physiol Cell Physiol 2010; 299:C606–C613.
45. Spindler V, Meir M, Vigh B, Flemming S, Hutz K, Germer CT, Waschke J, Schlegel N. Loss of desmoglein 2 contributes to the pathogenesis of Crohn's disease. Inflamm Bowel Dis 2015;21:2349–2359.
46. Ellawindy A, Satoh K, Sunamura S, Kikuchi N, Suzuki K, Minami T, Ikeda S, Tanaka S, Shimizu T, Enkhjargal B, Miyata S, Taguchi Y, Handoh T, Kobayashi K, Kobayashi K, Nakayama K, Miura M, Shimokawa H. Rho-kinase inhibition during early cardiac development causes arrhythmogenic right ventricular cardiomyopathy in mice. Arterioscler Thromb Vasc Biol 2015;35:2172–2184.
47. Citi S, Guerrera D, Spadaro D, Shah J. Epithelial junctions and Rho family GTPases: the zonular signalosome. Small GTPases 2014;5:e973760.
48. Viswanathan VK, Lukic S, Koutsouris A, Miao R, Muza MM, Hecht G. Cytokeratin 18 interacts with the enteropathogenic *Escherichia coli* secreted protein F (EspF) and is redistributed after infection. Cell Microbiol 2004;6:987–997.
49. Hernández-Nava E, Cuellar P, Nava P, Chávez-Munguía B, Schnoor M, Orozco E, Betanzos A. Adherens junctions and desmosomes are damaged by *Entamoeba histolytica*: participation of EhCPADH complex and EhCP112 protease. Cell Microbiol 2017;19:e12761.
50. Maia-Brigagão C, Morgado-Díaz J, De Souza W. *Giardia* disrupts the arrangement of tight, adherens and desmosomal junction proteins of intestinal cells. Parasitol Int 2012;61:280–287.
51. Wine E, Chan VL, Sherman PM. *Campylobacter jejuni* mediated disruption of polarized epithelial monolayers is cell-type specific, time dependent, and correlates with bacterial invasion. Pediatr Res 2008;64:599–604.
52. Aktories K. Rho-modifying bacterial protein toxins. Pathog Dis 2015;73:ftv091.
53. Ahrens S, Geissler B, Satchell KJ. Identification of a His-Asp-Cys catalytic triad essential for function of the Rho inactivation domain (RID) of *Vibrio cholerae* MARTX toxin. J Biol Chem 2013;288:1397–1408.
54. Prehna G, Ivanov MI, Bliska JB, Stebbins CE. *Yersinia* virulence depends on mimicry of host Rho-family nucleotide dissociation inhibitors. Cell 2006;126: 869–880.
55. Shawki A, McCole DF. Mechanisms of intestinal epithelial barrier dysfunction by adherent-invasive *Escherichia coli*. Cell Mol Gastroenterol Hepatol 2017; 3:41–50.
56. Singh AP, Aijaz S. Enteropathogenic *E. coli*: breaking the intestinal tight junction barrier. F1000Res 2015; 4:231.
57. Guttman JA, Kazemi P, Lin AE, Vogl AW, Finlay BB. Desmosomes are unaltered during infections by attaching and effacing pathogens. Anat Rec (Hoboken) 2007; 290:199–205.
58. Bulgin RR, Arbeloa A, Chung JC, Frankel G. EspT triggers formation of lamellipodia and membrane ruffles through activation of Rac-1 and Cdc42. Cell Microbiol 2009;11:217–229.
59. Arbeloa A, Blanco M, Moreira FC, Bulgin R, Lopez C, Dahbi G, Blanco JE, Mora A, Alonso MP, Mamani RC, Gomes TA, Blanco J, Frankel G. Distribution of *espM* and *espT* among enteropathogenic and enterohaemorrhagic *Escherichia coli*. J Med Microbiol 2009; 58:988–995.
60. Arbeloa A, Garnett J, Lillington J, Bulgin RR, Berger CN, Lea SM, Matthews S, Frankel G. EspM2 is a RhoA guanine nucleotide exchange factor. Cell Microbiol 2010; 12:654–664.
61. Mundy R, MacDonald TT, Dougan G, Frankel G, Wiles S. *Citrobacter rodentium* of mice and man. Cell Microbiol 2005;7:1697–1706.
62. Ritchie JM, Waldor MK. The locus of enterocyte effacement-encoded effector proteins all promote enterohemorrhagic *Escherichia coli* pathogenicity in infant rabbits. Infect Immun 2005;73:1466–1474.
63. Myhal ML, Laux DC, Cohen PS. Relative colonizing abilities of human fecal and K 12 strains of *Escherichia coli* in the large intestines of streptomycin-treated mice. Eur J Clin Microbiol 1982;1:186–192.
64. Taylor J. Infectious infantile enteritis, yesterday and today. Proc R Soc Med 1970;63:1297–1301.
65. Levine MM, Nataro JP, Karch H, Baldini MM, Kaper JB, Black RE, Clements ML, O'Brien AD. The diarrheal response of humans to some classic serotypes of enteropathogenic *Escherichia coli* is dependent on a plasmid encoding an enteroadhesiveness factor. J Infect Dis 1985;152:550–559.
66. Kenny B, Lai LC, Finlay BB, Donnenberg MS. EspA, a protein secreted by enteropathogenic *Escherichia coli*, is required to induce signals in epithelial cells. Mol Microbiol 1996;20:313–323.

Received September 9, 2017. Accepted April 20, 2018.

Correspondence
Address correspondence to: V. K. Viswanathan, PhD, School of Animal and Comparative Biomedical Sciences, 1006 E. Lowell, Building 106, Room 231, University of Arizona, Tucson, Arizona 85721. e-mail: vkv@email.arizona.edu; fax: (520) 621-6366.

Acknowledgments
The authors thank Professor Mrinalini Rao for critically reading the manuscript and suggesting substantial improvements. The authors also thank Anthony

Joseph Santiago for assisting with the animal experiments. The authors gratefully acknowledge the University of Arizona Microscopy Alliance for providing access to their FEI Tecnai Spirit 120kV Transmission Electron Microscope and DeltaVision Elite Deconvolution Microscope, and William Day, Patricia Jansma, and Allison Buchanan for technical support.

Author contributions

Jennifer Lising Roxas was involved in data acquisition, analysis, interpretation, and drafting the manuscript; V. K. Viswanathan was responsible for funding, the study concept, and design; Gayatri Vedantam was involved in the study design, and critical revision of the manuscript for important intellectual content; James B. Kaper contributed key resources and strains for the study; Bryan Angelo P. Roxas assisted with manuscript preparation and statistical analysis; Al B. Agellon assisted with image acquisition; and Ross Calvin Monasky and Asad Mansoor facilitated data acquisition for some experiments.

Conflicts of interest

The authors disclose no conflicts.

Funding

This work was supported by National Institutes of Health grant NIAID1R01AI081742 (V.K.V.). Work in Dr Viswanathan's laboratory also is supported by the United States Department of Agriculture Co-op Research and Extension Services (USDA CSREES) Hatch Program (ARZT-5704100-A02-140). Work in Dr Vedantam's laboratory is funded by grant 1I01BX001183-01 from the US Department of Veterans Affairs and grant ARZT-570410-A-02-139 from the United States Department of Agriculture Co-op Research and Extension Services (USDA CSREES) Hatch Program (G.V.). The University of Arizona Microscopy Alliance provided access to their FEI Tecnai Spirit 120kV Transmission Electron Microscope (supported by National Institutes of Health grant 1S10OD011981-01).